CHARGED PARTICLE MEASUREMENTS ON A 30-CM DIAMETER MERCURY ION ENGINE THRUST BEAM

J. M. Sellen, Jr., G. K. Komatsu, D. K. Hoffmaster, and R. F. Kemp

25781-6001-RU-00

1 April 1974

Contract No. NAS3-17641

TRW Systems
One Space Park
Redondo Beach, California 90278

CHARGED PARTICLE MEASUREMENTS ON A 30-CM DIAMETER MERCURY ION ENGINE THRUST BEAM

J. M. Sellen, Jr., G. K. Komatsu, D. K. Hoffmaster, and R. F. Kemp

1. INTRODUCTION

This technical memorandum will report a series of measurements of both thrust ions and charge exchange ions in the beam of a 30 centimeter diameter electron bombardment mercury ion thruster. A qualitative model will also be presented which describes magnitudes of charge exchange ion formation and motions of these ions in the weak electric field structure of the neutralized thrust beam plasma. Areas of agreement and discrepancy between observed and modeled charge exchange properties will be discussed.

2. ION THRUSTER AND DIAGNOSTIC PROBE ARRAY

The 30-cm ion thruster was mounted in a 5' x 10' testing chamber with liquid nitrogen cooled shrouds and beam collector. Both shrouds and the collector are electrically isolated from each other and the chamber ground and were floating during thrust beam operation, thus requiring neutralization of the thrust beam by a plasma discharge neutralizer.

The ion engine and the array of Faraday cups used in the experiments are illustrated in Figure 1. The "1-meter" J_+ measures ion current density in a plane 1 meter from the accelerator grid plane. The probe may be moved in the radial direction from the thrust beam axis to ∿70 centimeters from the axis, which allows a measurement of ions moving at angles with respect to the beam axis from 0° to ∿35°. The 1-meter J_+ is gridded, as are all probes, to prevent electron passage from the thrust plasma to the cup collector, and to suppress secondary electrons emitted from the cup collector under energetic ion impact.

The "swinging J" moves along the arc of a 62 centimeter radius circle whose center of curvature is at the intersection of the beam axis

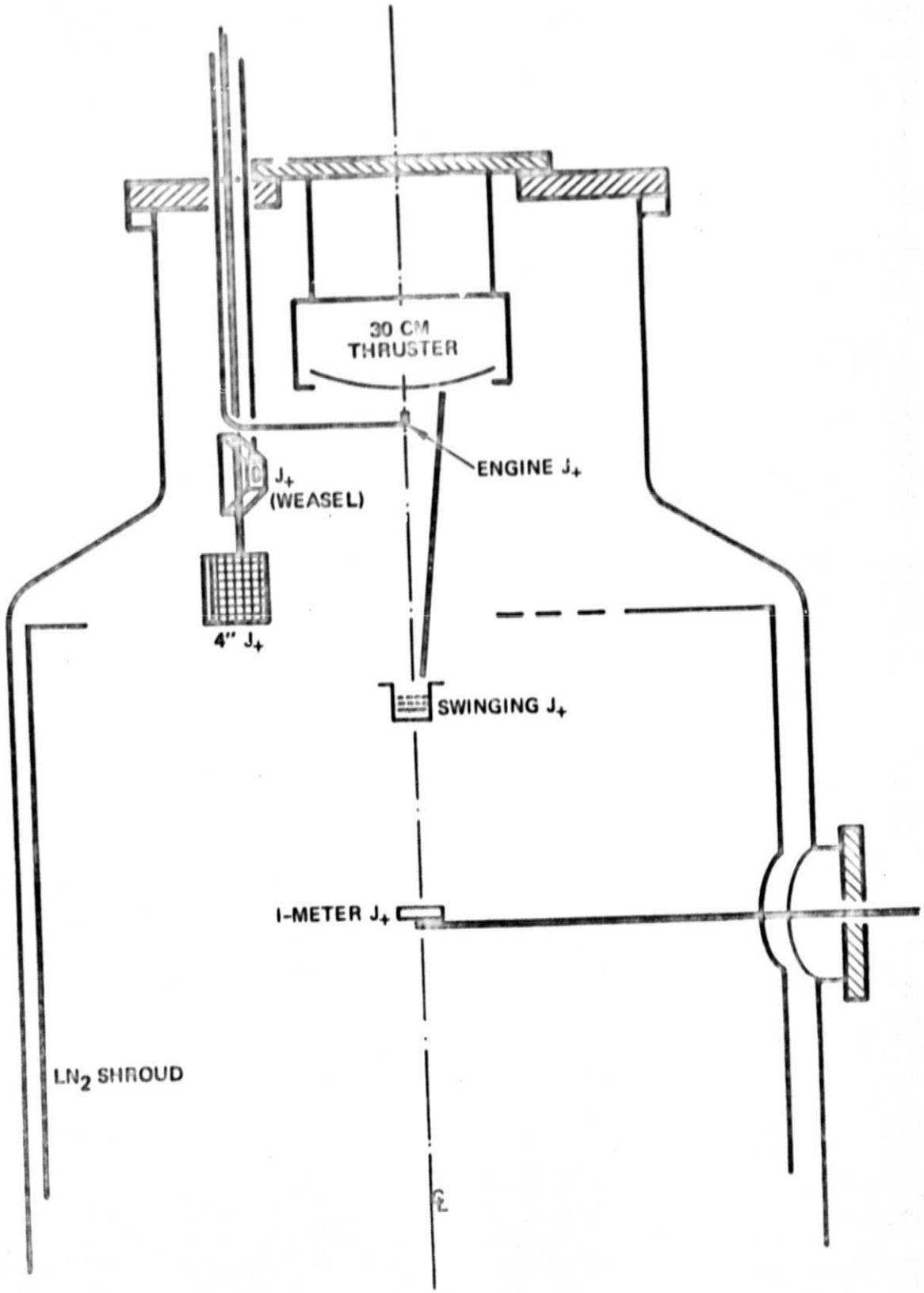

Figure 1. Diagram of experimental facility indicating ion engine and diagnostic array.

with the accelerator grid. Measurements of ion current density can be made for ions moving at divergence angles from the thrust beam axis from 0° to 60°. The swinging J_+ Faraday cup is also provided with an additional grid so that retarding potential analyses can be performed on lower energy ions.

The "engine J_+" is a small Faraday cup (∿0.6 centimeter aperture diameter) which swings along a circular arc of 34.3 centimeters radius. The arc of this circle intersects the thrust beam axis. The probe may also be moved in the axial (z) direction, and permits a two dimensional determination (r, z), of thrust ion current density from the accelerator grid plane to an axial distance of ∿20 centimeters.

The "4" J_+" is a multigridded Faraday cup which may be moved axially and may also be rotated about its supporting rod. In the measurements described in this memoranda, the normal to the cup collector surface passes through the thrust beam axis. The principal use of this Faraday cup is a measure of ion current density as a function of axial position along a cylinder of 34 centimeters radius (cylinder axis and thrust beam axes coincide). Because of cup and grid construction, ion detection results for ions moving over a cone of directions from zero to ∿90° with respect to the collector surface normal. This "total ion current" probe also contains an additional grid for retarding potential analyses.

A final Faraday cup in the array is the "weasel J_+", so named for the several degrees of freedom in the probe motion. The weasel J_+ is a multicollector (5), multigridded (2) probe which allows determination of charge exchange ion current density as functions of emergence angle (relative to the thrust axis) and axial position (along a cylinder of 34 cm radius with cylinder axis and thrust axes coinciding). For the experiments described in this report, probe motion used only the z variation, and probe orientation was such that normals to the collecting surfaces passed through the thrust axis.

3. THRUST ION CURRENT DENSITY MEASUREMENTS

3.1 1 Meter J_+

Figure 2 illustrates the relative Faraday probe cup current as a function of radial position at 1 meter from the accelerator grid plane. The

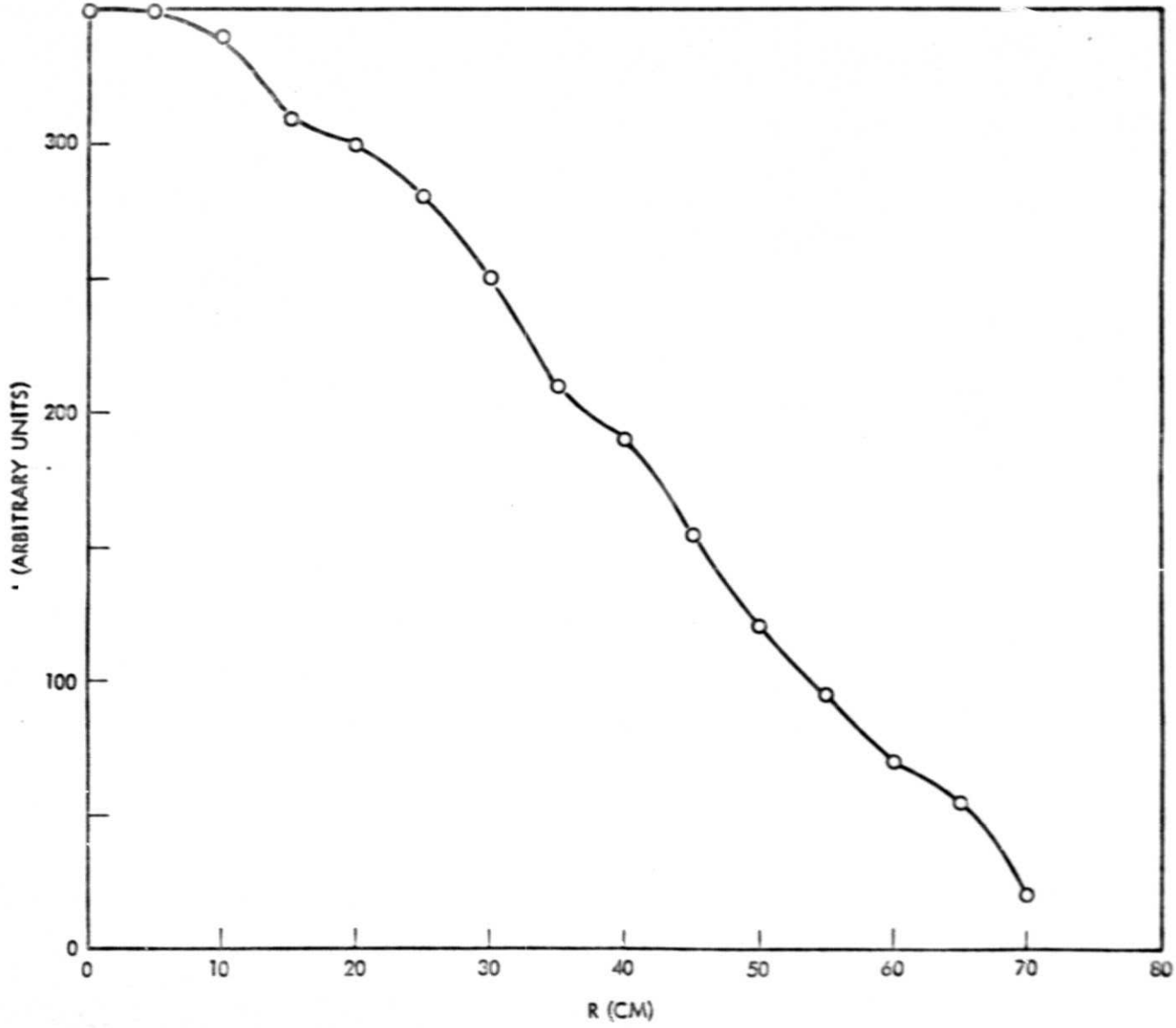

Figure 2. Relative ion current density profile at z = 1 m.

ion current density profile illustrated is comparatively broad, reflecting the use of a dished grid system ("outward" dishing), equal hole areas in both screen and accelerator grids, and the use of uncompensated grids. Because finite level current densities are still present at r = 70 centimeters ($\theta \sim 35°$), computations of the average ion divergence angle, $\langle\theta\rangle$, were not carried out with this data.

3.2 Swinging J_+

Figure 3 illustrates thrust ion current density as a function of divergence angle from 0 to 60°. For this 1 ampere beam condition, the average angle of ion divergence is ∿30°, and $\langle\cos\theta\rangle = 0.843$. The value of the thrust factor here is similar to results reported by Danilowicz, Rawlin, Banks, and Wintucky[1] for uncompensated grids and with equal screen and accelerator grid hole sizes ("F1" conditions). Thus, while the present beam is divergent, it is not unrepresentative of uncompensated grids, and can be used to determine qualitative features of the charge exchange ion formation and deposition patterns.

3.3 Engine J_+

Figure 4 illustrates the relative values of Engine J_+ Faraday cup current as a function of rotation angle, α, of the probe about its supporting shaft. The scan illustrated there is at z = 6.3 centimeters. For $\alpha = 90°$, the probe is on the beam axis, and, since the rotation arm length is 34.3 centimeters, radial position in the beam is given by

$$r = 68.6 \sin \frac{\alpha}{2} \text{ centimeters} \quad . \tag{1}$$

These probe scans were repeated with stepwise variation of z through the range from $6 < z < 24$ centimeters to provide the (r,z) thrust ion current density plots given in Section 5.1.

Also given in Figure 4 is the floating potential of the probe when the outer cap and collector elements are connected together and allowed to float across the 1 megohm input impedance of the recorder. The thrust beam potential is comparatively flat and is very nearly the value of potential on the keeper electrode for the discharge neutralizer. These features indicate an effective coupling of the discharge neutralizer to the thrust beam plasma

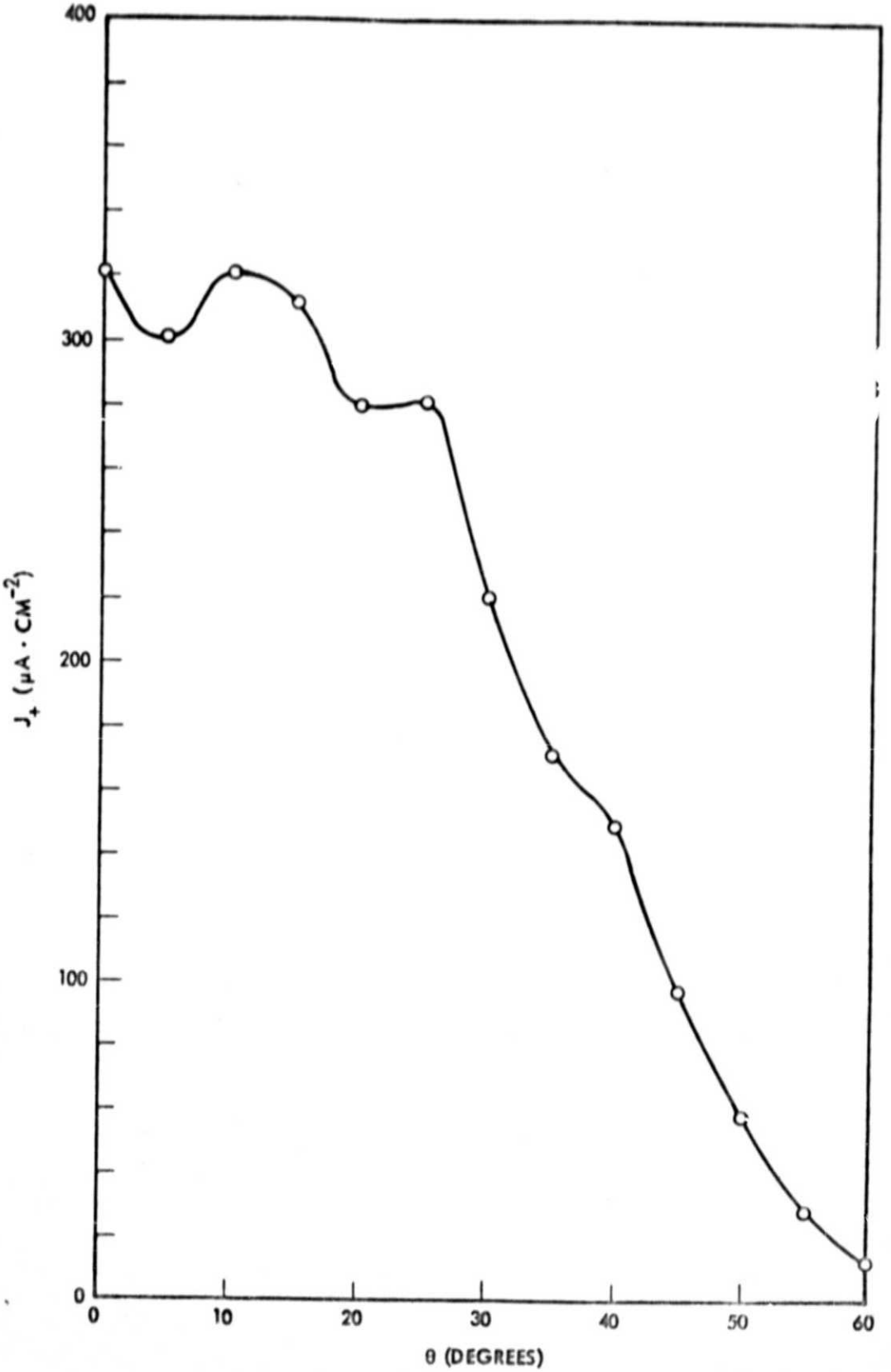

Figure 3. Ion current density profile obtained from swinging J_+ Faraday cup data.

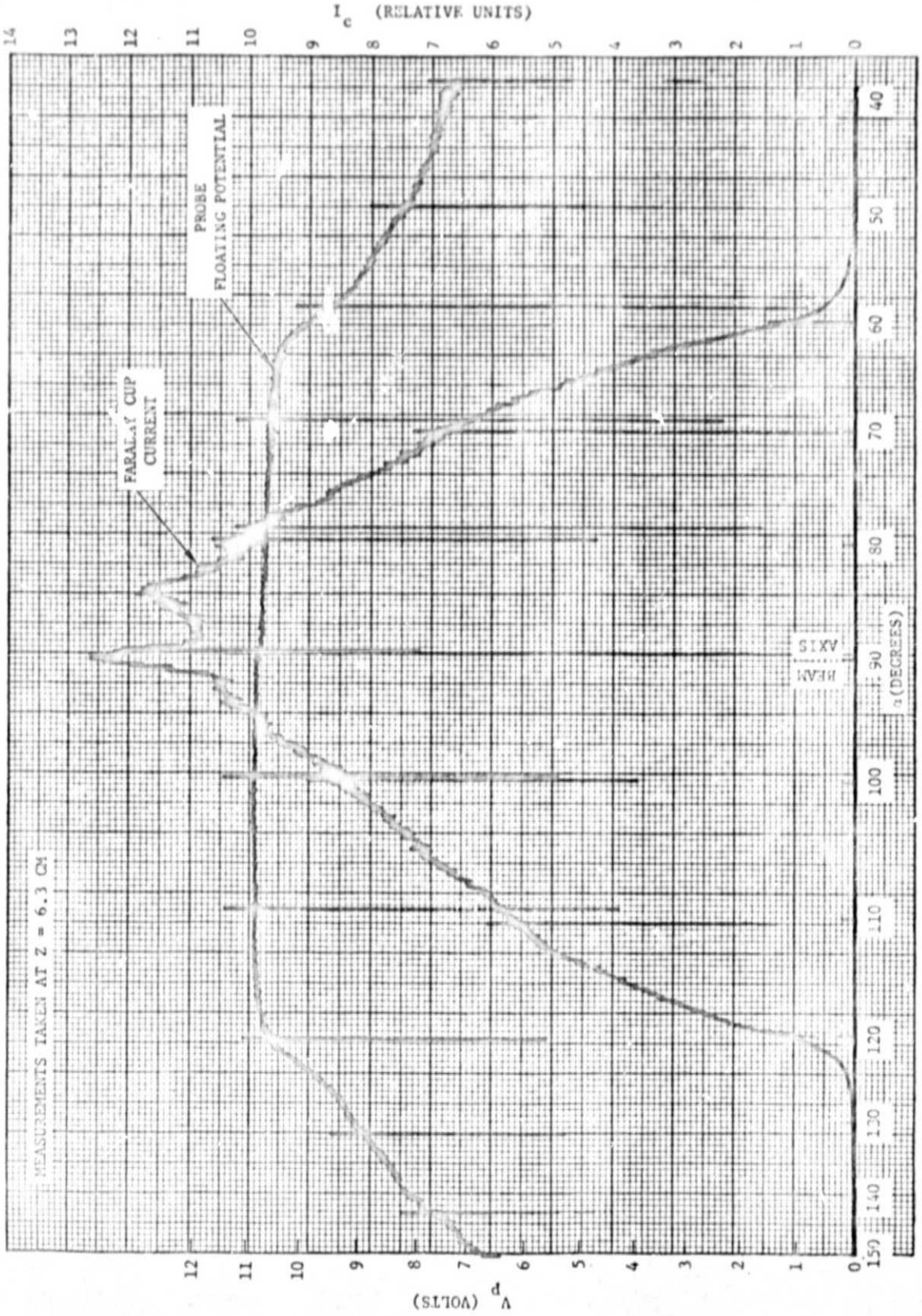

Figure 4. Probe floating potential and relative ion current density profile utilizing the engine J_+ Faraday cup.

(small injection potential) and a "small" value of thrust beam neutralizing electron temperature (flatness of probe floating potential in the presence of thrust plasma density gradients: see also Section 5.1). The more rapid variations in probe floating potential for $\alpha < 60°$ and $\alpha > 120°$, are the result of comparatively large plasma density gradients and diminished capability of the intercepted ion current to drive the input impedance of the floating probe (1 megohm requires 1 μampere of intercepted ion current per volt of floating potential). Electric fields in the boundaries of the thrust beam plasma cannot be accurately determined from observed variations in probe floating potential, and the electric fields used in the charge exchange ion trajectory calculations in Section 5.1 for motion inside the thrust beam have been based upon measured thrust beam density, the Boltzmann relationship between potential, density, and electron temperature, and an assumed value of T_e, electron temperature.

4. CHARGE EXCHANGE ION MEASUREMENTS

4.1 General

The use of retarding potential analyses can determine the kinetic energy of a charged particle and, by inference, the value of the potential at the point of formation of the particle. While this procedure effectively separates charge exchange ions from more energetic thrust beam particles, the Faraday cups are not mass specific and hence cannot determine whether the charge exchange particle is Hg^+ or, perhaps, a charge exchange metal ion from a sputtered engine electrode atom. In later discussion (Section 7) it will be shown that the most likely possibility, by far, is that the charge exchange ions observed are Hg^+, and, in the treatment throughout this report, this will be the assumed condition.

4.2 4" J_+ Measurements

For the 1-meter J_+, the swinging J_+, and the engine J_+, thrust ion current densities are very much larger than charge exchange ion current densities, and retarding potential analyses by these probes, where possible, reveal no significant low energy ion component fraction. The 4" J_+ and the weas J_+ are removed from the thrust beam, however, and examine ions at

comparatively high divergence angles and are, thus, located in spatial and angular regions where low energy particles are significant fractions of observed currents.

The 4" J_+ has two grids over the collecting surface, and, by selective variations of axial position and/or potential applied to the grids, the doubly differentiated distribution of ions (with respect to position and energy) may be determined. Figure 5 illustrates the results of such a double differentiation process. At the upper left of the figure, the current density of all ions is given as a function of z (z = 0 is the plane of the accelerator grid) along the cylinder at r = 34.3 centimeters and whose axis coincides with the thrust beam axis. At the lower right of the figure is the current density of ions whose energy exceeds 30 electron volts, and other curves illustrate other lower energy cutoffs.

Several features of these histograms are of interest. The first is the "noise" introduced into the histograms height through the processes of double differentiation. In spite of this noise, however, it is evident that charge exchange ions exist (diminutions in current for retarding potentials advancing through the 6 to 12 volt region, which includes the potential of the thrust beam in which the charge exchange ion is formed), that "energetic" ions exist (not affected by 30 volts retardation) at angles up to ~90° of divergence angle, and that charge exchange current densities appear, if anything, to increase for increasing z (compare differential histogram heights at 0 and 30 volts retardation voltage for z = 5 and z = 10 centimeters).

While the data from this probe, as illustrated in Figure 5, reveals several features of the charge exchange ions and energetic high angle ions, magnitudes of charge exchange ion space charge created problems of ion transmission in the grid system used in this probe ("premature" cutoff) and subsequent determinations of charge exchange ions were made with the weasel, J_{+W}.

4.3 Weasel J_+ Measurements

A cross section of the J_{+W} probe is given in Figure 6. The probe consists of 5 separate collectors which have, in combination with the probe entrance aperture, angular ranges as indicated in the figure. The collectors

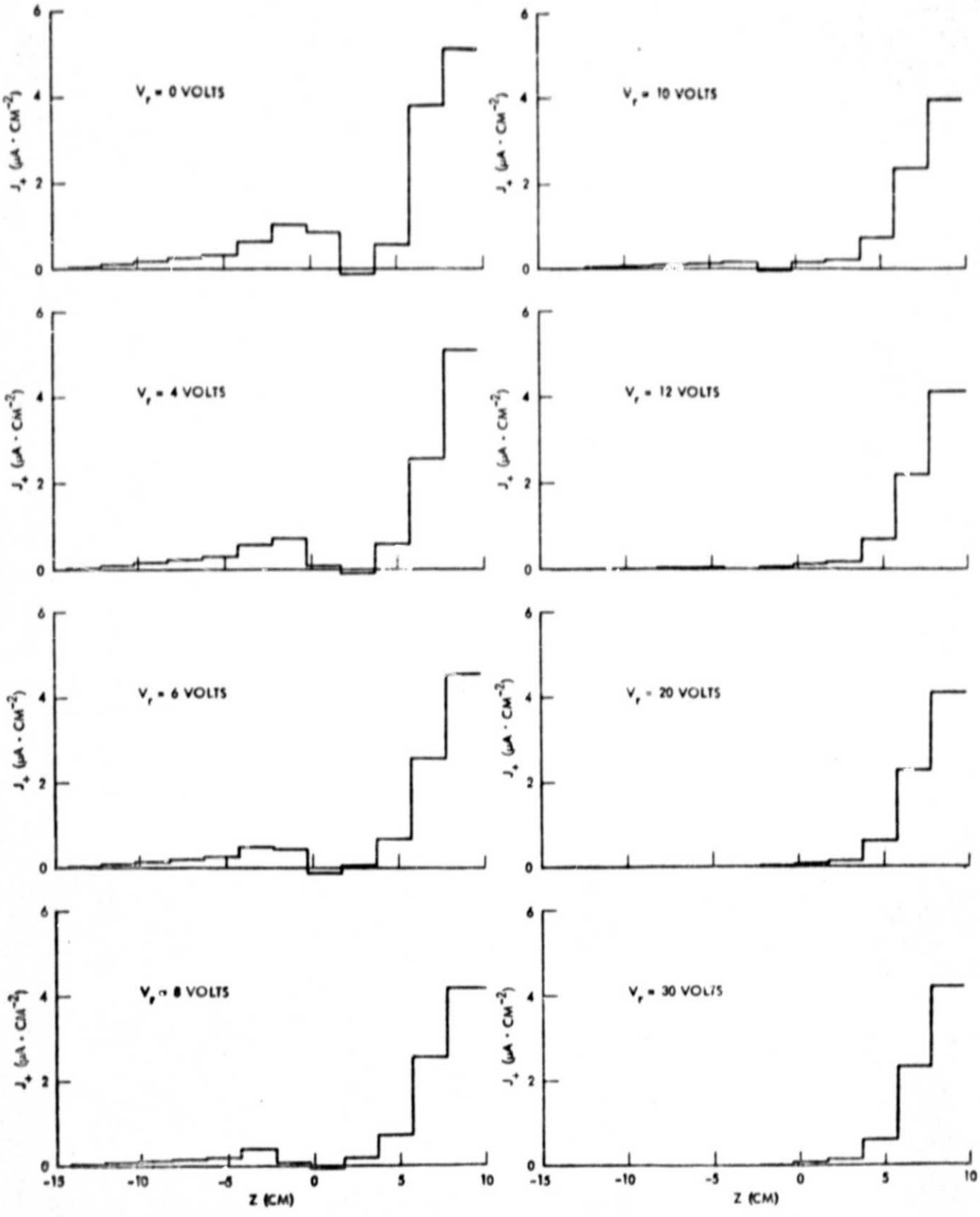

Figure 5. Ion current density as a function of axial distance (z) and retarding potential (V_r) along the cylinder at r = 32 cm for the 4" J_+ probe.

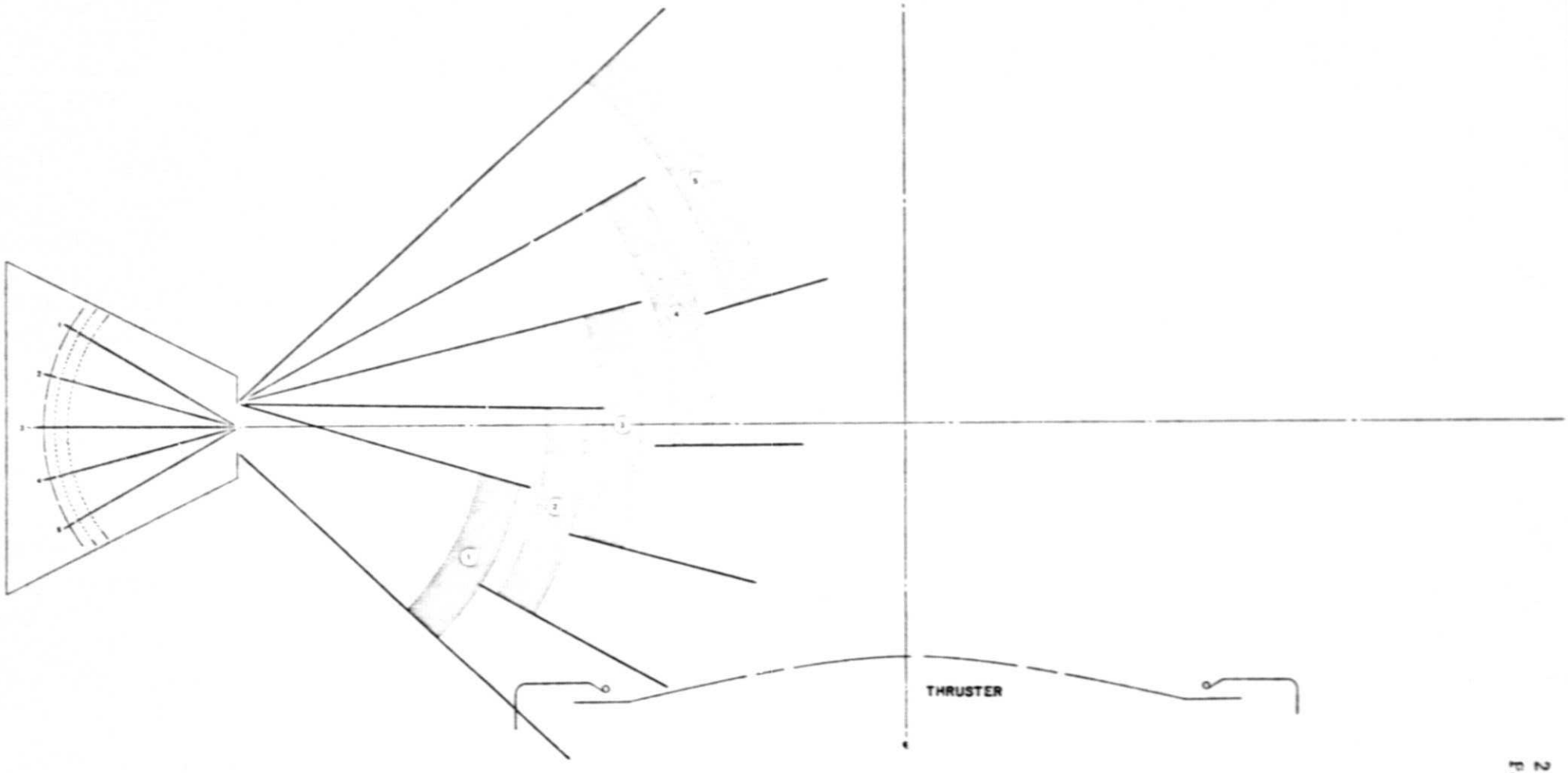

Figure 6. Cross-section of the J_{+W} probe and its spacing relative to the thrust beam axis. Axial motion is $-1 < z < 26$ cm. Channel angular midpoints are at $\theta = 60°$, 75°, 90°, 105°, and 120°. Effective angular acceptance ranges are indicated.

are behind a double grid. In practice the forward grid is set at zero potential and the middle grid is set at various positive potential biases to perform the retarding potential analysis. The thrust beam axis is indicated in the figure and the probe motion is parallel to this axis. The angular separation from collector-to-collector is 15° and the effective angular width of a channel is 15°. The center lines of the channels range from $\theta = 60°$ (channel 1) to $\theta = 120°$ (channel 5).

When the center line of J_{+W} is placed at z = 2.1 centimeters, and retarding potential is varied from 0 to 25 volts, the differential currents with respect to retardation potential given in Figure 7 are obtained. For this engine operation condition, the keeper voltage was set at 11 volts, and the sharp peaking of the ion energy distribution curves at retarding potentials in the range from 8 to 12 volts is clear evidence of formation of these ions through charge exchange in the thrust beam plasma. The ions appear to be broadly distributed in angle, with perhaps larger magnitudes at 60° than 120°. The shift in the $\Delta I_c/\Delta V_r$ peak in channel 4 from the peaks observed in other channels is probably an instrumental, rather than a real, effect.

The display of $\Delta I_c/\Delta V_r$ which shows large signal levels near V_r = 8-12 volts, is not effective in illustrating energetic high angle ions. These ions were present, during the basic data run, but differentiation with respect to V_r yields very small signals in that there are no appreciable shifts in recorded currents for variation of V_r in this low range. Variation of V_r into the range of several hundred volts does, however, cause a diminution of high angle high energy ion currents.

When the J_{+W} is moved in the z direction and retardations are used to distinguish charge exchange ions from thrust ions, the currents in all channels sum to the levels illustrated in Figure 8. There the distinct peaking in thrust ion currents can be identified as ions streaming from the engine in the range from 60° to 90° (channels 1 and 2 primarily, with smaller signals in channel 3). The currents of charge exchange ions, summed over all channels, illustrates a rising level for increasing z, thus confirming earlier indications of z dependence of these currents obtained with the 4" J_+. The slight drop in

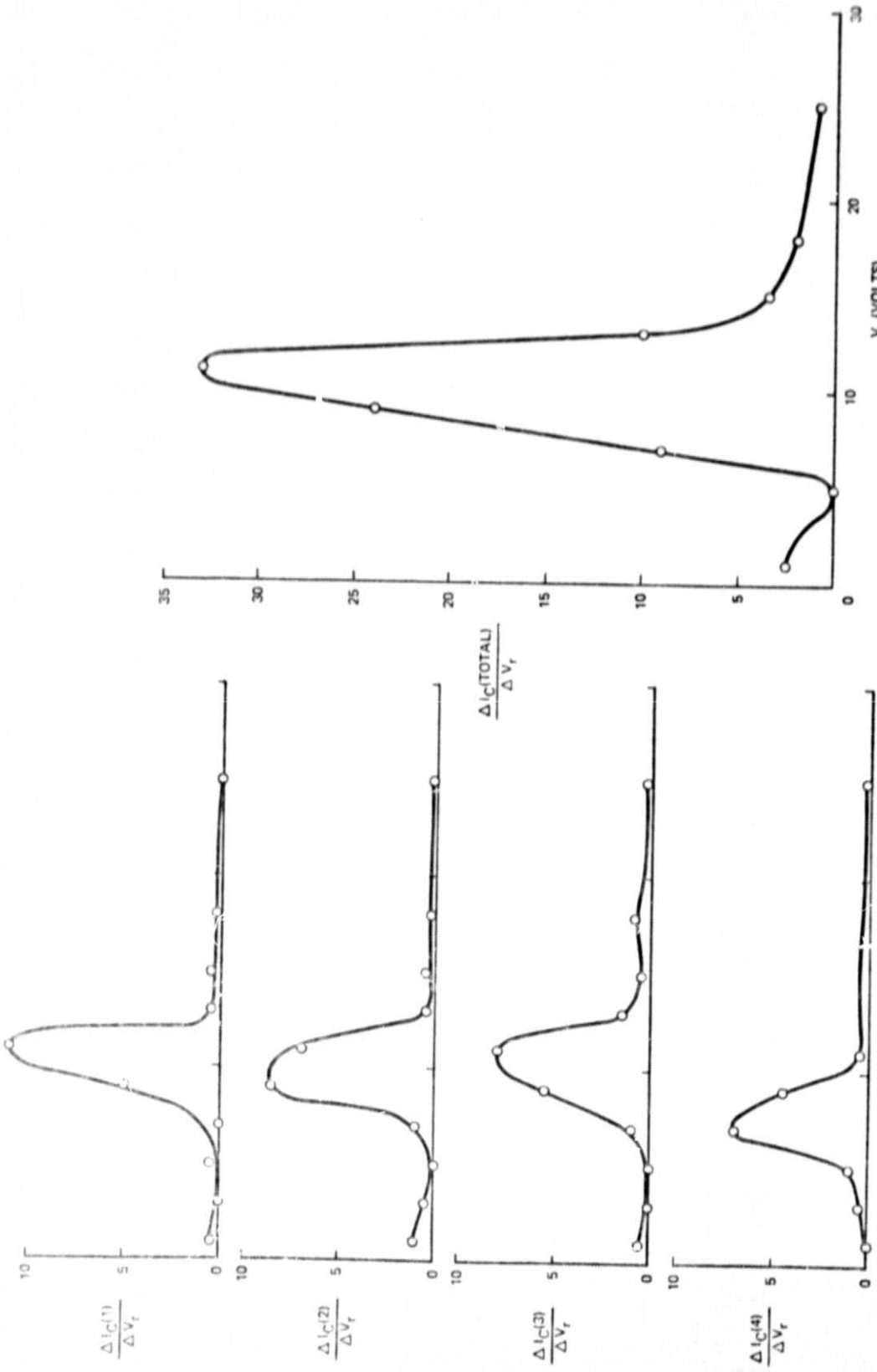

Figure 7. Differential ion current as a function of retardation voltage for J_{+W} channels individually and summed. Neutralizer keeper potential was 11 volts. J_{+W} probe was at z = 2.1 cm.

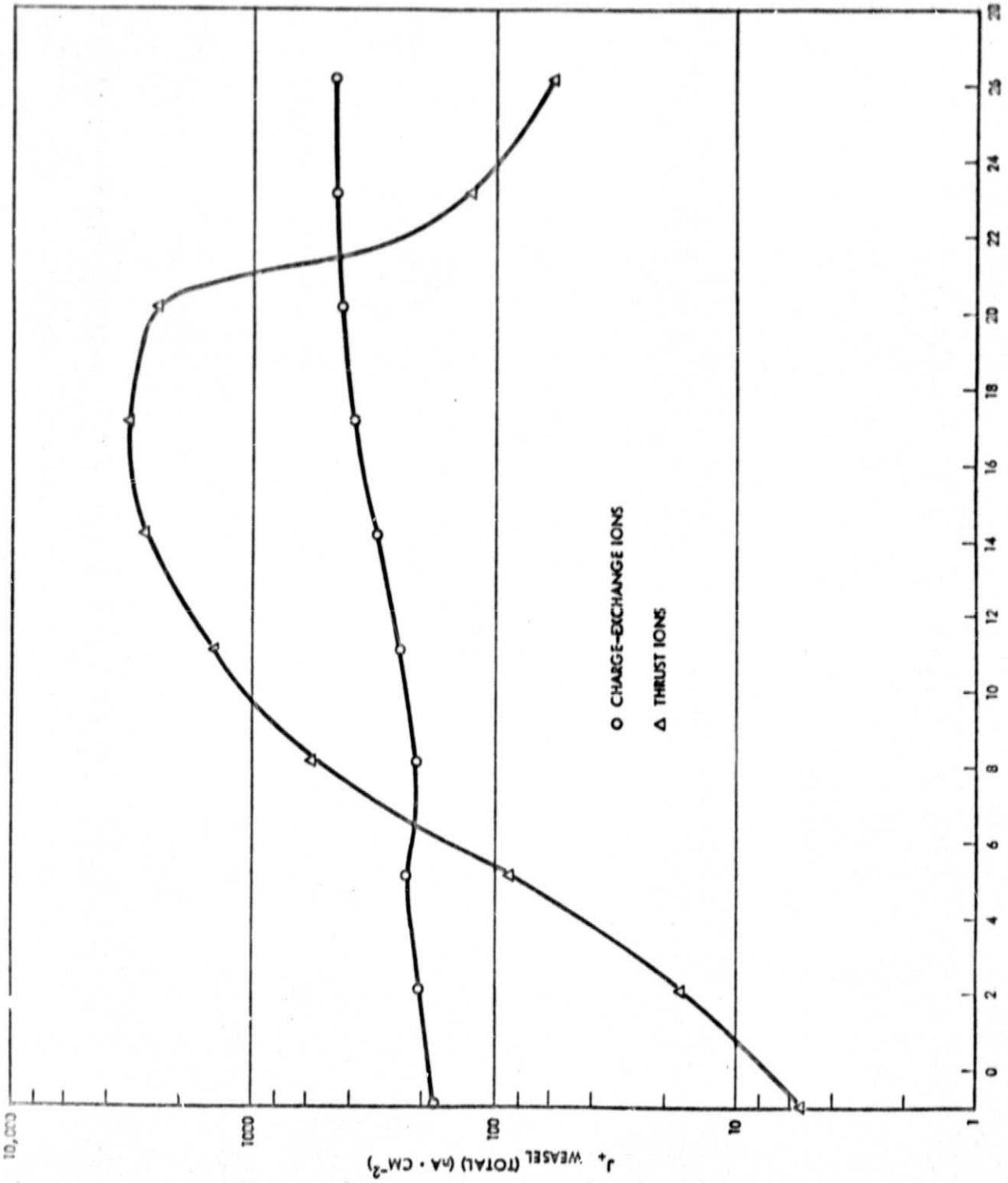

Figure 8. Charge exchange ions ($eV_+ < 30$ eV) and thrust beam ions summed over all J_{+W} channels as a function of axial position.

charge exchange signal as z moves from 5 to 7 centimeters is considered a result of secondary electron emission effects in the presence of strong currents of thrust ions. These effects are more pronounced in the data of the individual channels.

Figures 9-13 illustrate the z dependence of the charge exchange currents (energies less than 30 eV) in the various channels. The region from z = 5 to z = 20 centimeters is adversely affected by strong currents of thrust ions at $\theta = 60°$ which cause secondary emission at the collector surface. The initial increase of retarding potential on the middle grid (application of positive potential) causes an increased flow of secondary electrons from the collector to the grid. Since electron flow away from the collector is of the same polarity in signal as ion flow to the collector, the application of the positive bias causes increased collector signal and prevents the usual differential identification of charge exchange ions (loss of signal with increasing retardation). These effects are pronounced in channels 1 and 2 ($\theta = 60°$ and 75°), but are not of sufficient magnitude to affect charge exchange ion measurements in the remaining channels.

From Figure 9 it appears that the charge exchange signal is rising in the z range from 24 to 27 centimeters. For channel 2 the peak appears at $z \sim 20$ to 22 centimeters with slight decreases as z increases beyond this point. Similar effects are found in channels 3, 4, and 5. This behavior, apparently genuine, creates contradictions with what might be assumed in zero order, as an expected charge exchange ion deposition. The formation of charge exchange ions should proceed proportionally to the magnitudes of both thrust ion density and the density of neutral propellant atoms. The thrust ion density has an approximate form

$$\rho_+ \approx \frac{K_+}{(z + z_+)^2} \tag{2}$$

where z is the effective "source" point distance of a conical flow. Similar considerations apply to the density of neutrals

$$\rho_o \approx \frac{K_o}{(z + z_o)^2} \tag{3}$$

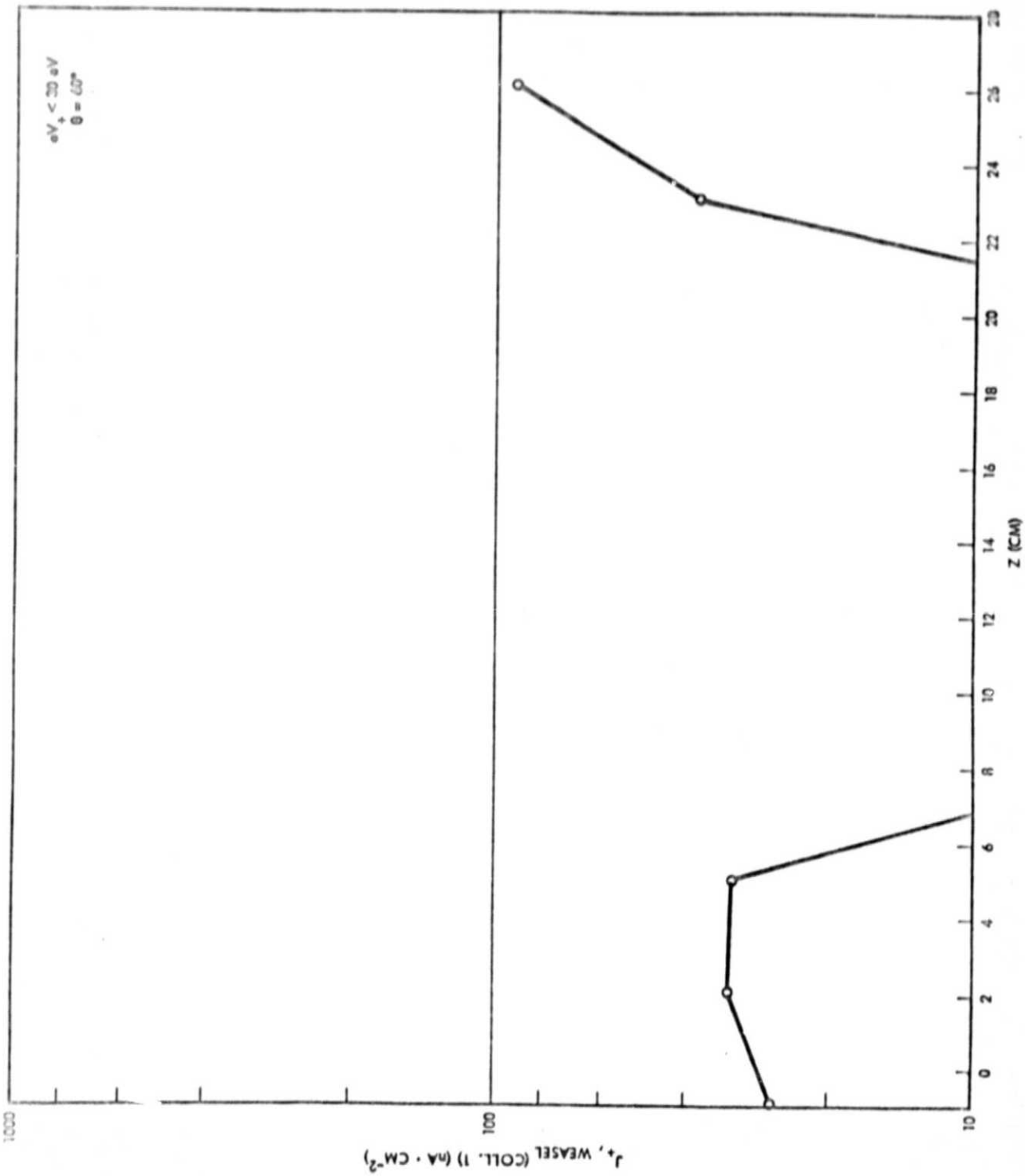

Figure 9. Charge exchange ion signal in channel 1 (θ = 60°) of J_{+W} probe as a function of axial position. Loss of signal in range 6 < z < 22 centimeters results from secondary electron effects due to large thrust ion signal levels.

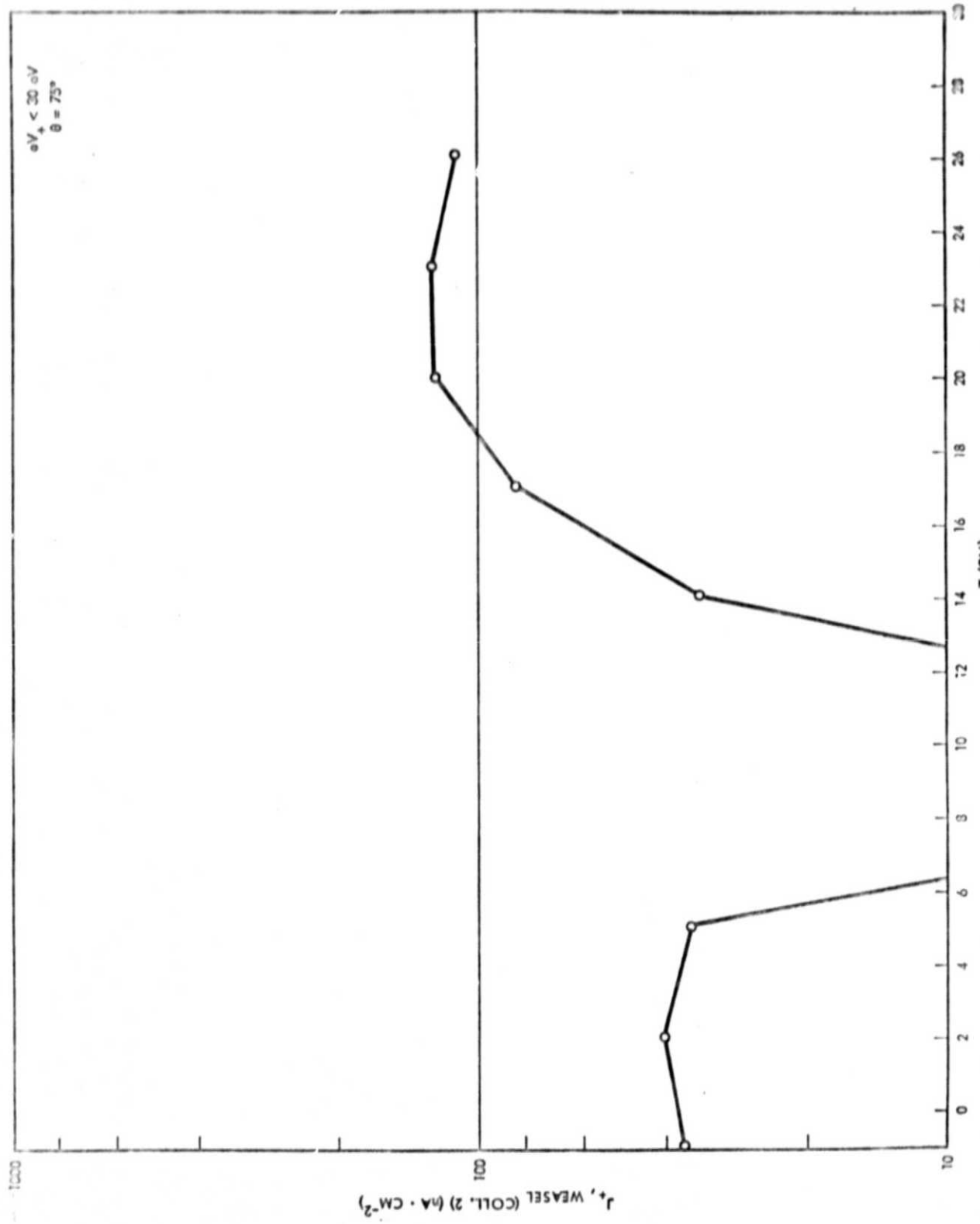

Figure 10. Charge exchange ion signal in channel 2 ($\theta = 75°$) of J_{+W} probe as a function of axial position. Loss of signal in range $6 < z < 14$ centimeters results from secondary electron effects due to large thrust ion signal level.

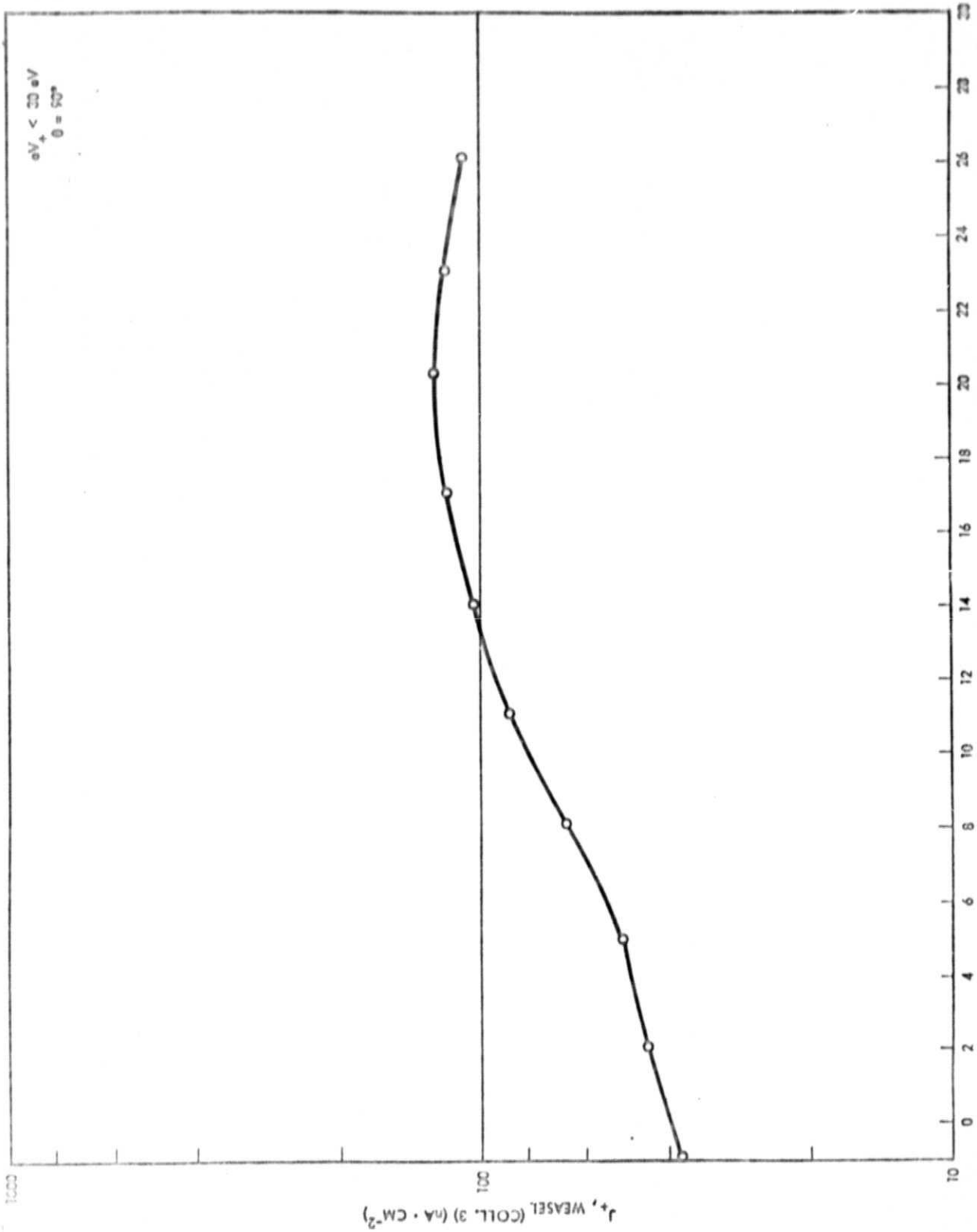

Figure 11. Charge exchange ion signal in channel 3 ($\theta = 90°$) of J_{+W} probe as a function of axial position.

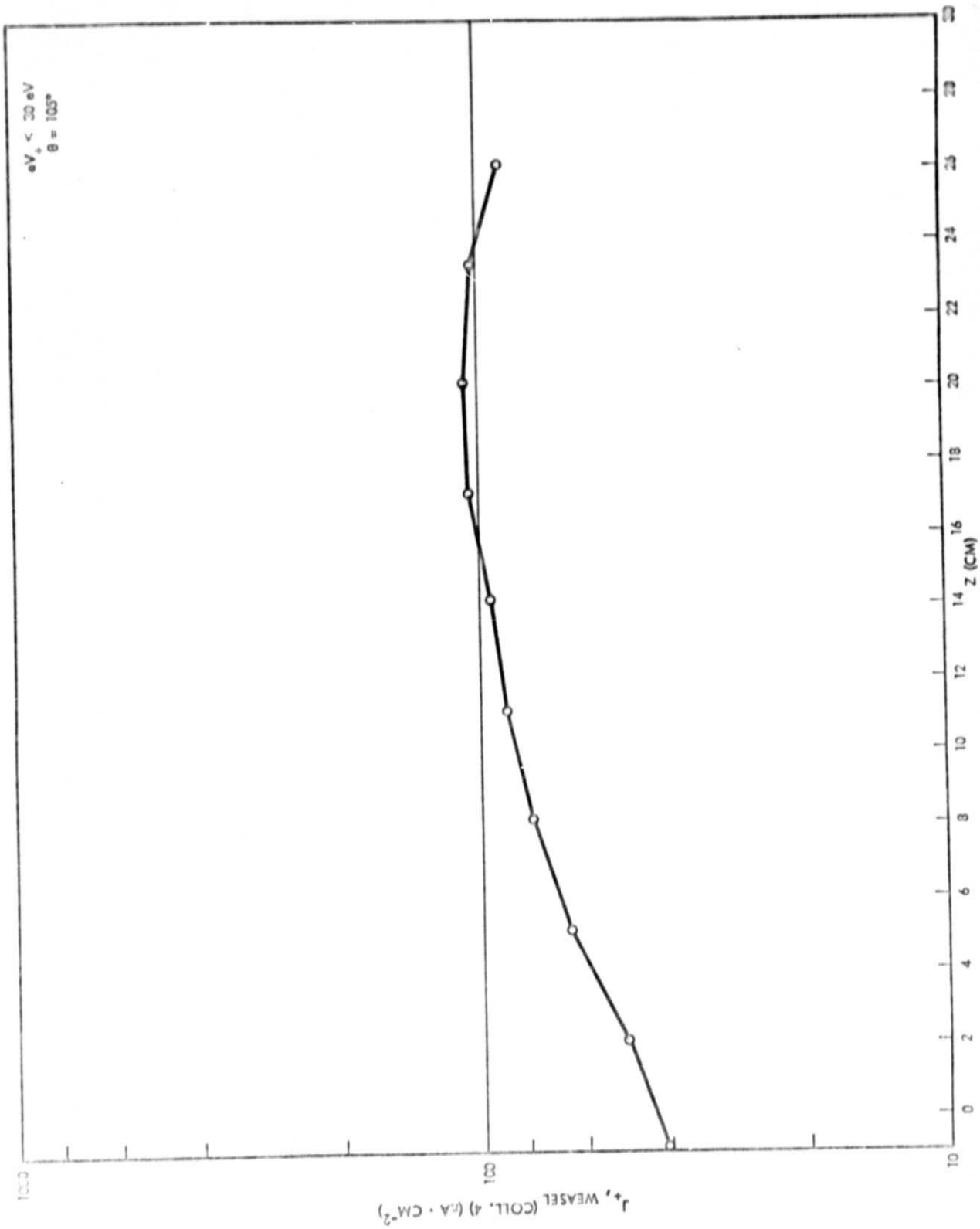

Figure 12. Charge exchange ion signal in channel 4 (θ = 105°) of J_{+W} probe as a function of axial position.

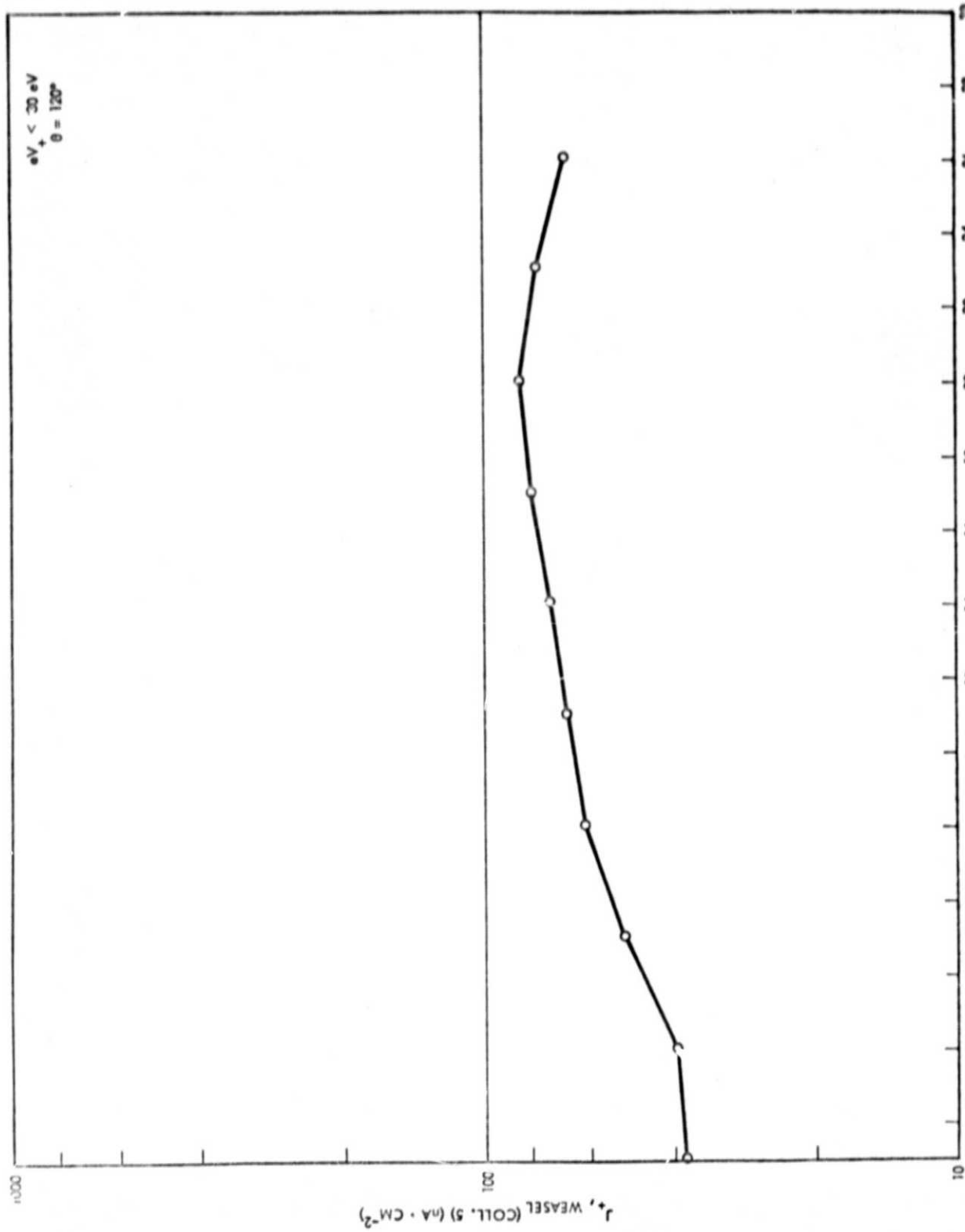

Figure 13. Charge exchange ion signal in channel 5(θ = 120°) of J_{+W} probe as a function of axial position.

where z_o may differ from z_+, since the total angles of the two "conical" beams may be expected to differ. The charge exchange ion formation rate will be given by

$$\frac{dn_{+,x}}{dt\,d(Vol)} = \frac{K_+ K_o}{(z + z_+)^2 (z + z_o)^2} \tag{4}$$

which has its maximum value for z = 0. If Eq. (4) is correct, however, then it would appear that $J_{+,x}$, the charge exchange ion current density should also be at maximum values for z = 0 rather than the observed results where peak $J_{+,x}$ is near z = 22 cm (for r = 34 cm). The resolution of this apparent contradiction is in the preferential drift of the ions, once formed, to larger values of z. This drift results from a weak electric field structure in the thrust beam, and Section 5 will derive expected forms of this field and will then view the possible motion of charge exchange ions as a result of $q\vec{E}$ forces.

5. MODELING OF CHARGE EXCHANGE ION PROPERTIES

5.1 Charge Exchange Ion Trajectories

The trajectory of a charge exchange ion will depend upon the initial velocity, $\vec{v}_o$, which the atom possessed at the instant of charge exchange, and the force, $q\vec{E}$, on the ion following charge exchange. Thus

$$\dot{z}(t) = \dot{z}(o) + \int_o^t qE_z dt \tag{5}$$

and

$$\dot{r}(t) = \dot{r}(o) + \int_o^t qE_r dt \tag{6}$$

denote ion z and r velocities at time t after ion formation, $\dot{z}(o)$ and $\dot{r}(o)$ are the atom z and r velocities at the instant of charge exchange and the indicated integrals in t must, of course, utilize the E_z and E_r experienced by the ion along its flight through the thrust beam. Eqs. (5) and (6) may be further extended to describe z(t) and r(t), through the indicated second stage of integration.

While Eqs. (5) and (6) are simple in principle, a practical evaluation will depend upon a complicated calculation, first of $\vec{E}$ and then of the particle motion in that $\vec{E}$ field. To evaluate the electric field the electrostatic "barometric" equation of the thrust beam may be utilized. This relation (essentially a Boltzmann law) states that

$$\rho_+ = \rho_o \exp \left\{ - eV_p/kT_e \right\} \tag{7}$$

where ρ_+ is plasma density, V_p is plasma potential, k is Boltzmann's constant, T_e is electron temperature in the plasma, e is the electron charge and potential at the maximum density point in the plasma ($\rho = \rho_o$) has been designated V = 0. From Eq. (6) it follows that V = constant for ρ_+ = constant. Thus, equidensity contours in the plasma become equipotential contours.

To determine the plasma equidensity contours, the engine J_+ data of the (r,z) behavior of ion current density is utilized. For a plasma beam in which the predominant species is thrust ions, the ion current density is given by

$$J_+ = \rho_+ v_{accel} \tag{8}$$

where v_{accel} is ion acceleration velocity. Measurement of J_+, thus, is a measurement of ρ_+.

The engine J_+ data of $J_+(r,z)$ is illustrated in Figure 14 over a range from 2.5 milliamperes/cm^2 to 0.05 milliamperes/cm^2.

The next step in the determination of $\vec{E}$ is to calculate the density gradients. From Eq. (7),

$$\vec{E} = - \frac{kT_e}{e} \left(\frac{1}{\rho_+} \right) \left(\frac{d\rho_+}{d\vec{s}} \right) \tag{9}$$

where $\vec{s}$ is the normal to an equidensity (equipotential) contour. These density gradient directions can be determined graphically from Figure 14, and the density gradients, $d\rho_+/ds$, may be calculated.

The final step in this process is the evaluation of kT_e. For the present experiments no Langmuir probe determinations of T_e were present.

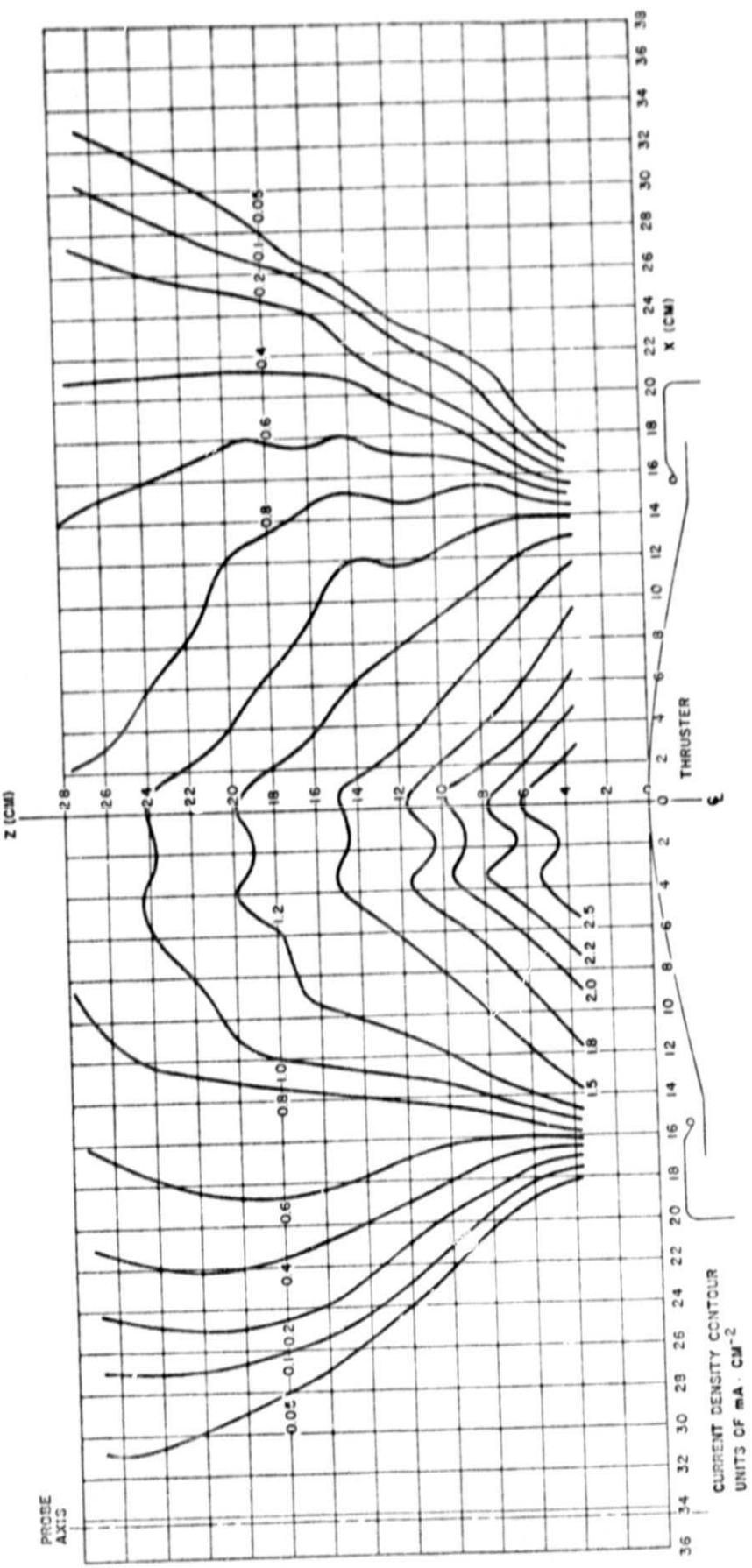

Figure 14. Thrust ion current density contours as a function of raidal and axial position from engine J_+ probe. Total ion beam current of 1.5 amperes.

However, the floating potential data illustrated in Figure 4 indicated an effective coupling and correspondingly low temperature value to T_e. In a series of measurements reported in reference 2, similarly neutralized thrust beams revealed $kT_e \approx 0.35$ electron volt (4000°K), and this value was used for the present modeling. From this assumed T_e, the measured densities, the calculated density gradients and Eq. (9), the electric field in the thrust beam may be computed. The resultant value and direction of this electric field is illustrated in Figure 15.

The calculation of trajectories has been carried out for a single point-of-origin of the charge exchange, but with three differing orientations of the initial velocity vector of the charge exchange ion. These trajectories are illustrated in Figure 16. In the calculations there it was assumed that the atom prior to charge exchange possessed a thermal velocity characteristic of a 500°K wall temperature. The initial orientations of this thermal velocity are $\theta = 0°$, 45°, and 60°. The result of the electric field in the thrust beam over the trajectory lengths indicated is to increase $\theta_o = 0$ to $\theta \sim 35°$, $\theta_o = 45°$ to $\theta \sim 72°$, and $\theta_o = 60°$ to $\theta \sim 83°$. Final to initial ion energies over the indicated trajectory lengths were 7.9, 17.4, and 18.1.

The calculations illustrated in Figure 16 do not cover, of course, all possible conditions on point of origin, or direction at origin. They do serve to illustrate, however, two features in the charge exchange ion motion. The first of these is the transport of the ion in the axial (as well as radial) direction and provides, thus, an explanation of the experimental observation of increasing deposition rates with increasing z (Section 4.3, J_{+W}). The second feature of the trajectories is the tendency toward increases in θ, and, from an examination of the E field structure in Figure 15, it would appear possible for a charge exchange ion to move initially in the +z direction, but, in the boundaries of the thrust beam, to encounter sufficient backwardly directed forces to result in a final velocity in the "backward" hemisphere. This result of the calculations would act to confirm the experimental observations of backwardly directed charge exchange ions at downstream values of z, (Figure 12 and 13). There is, thus, reasonable agreement between the general features of the experimental data and the computed properties of charge exchange ions in the model.

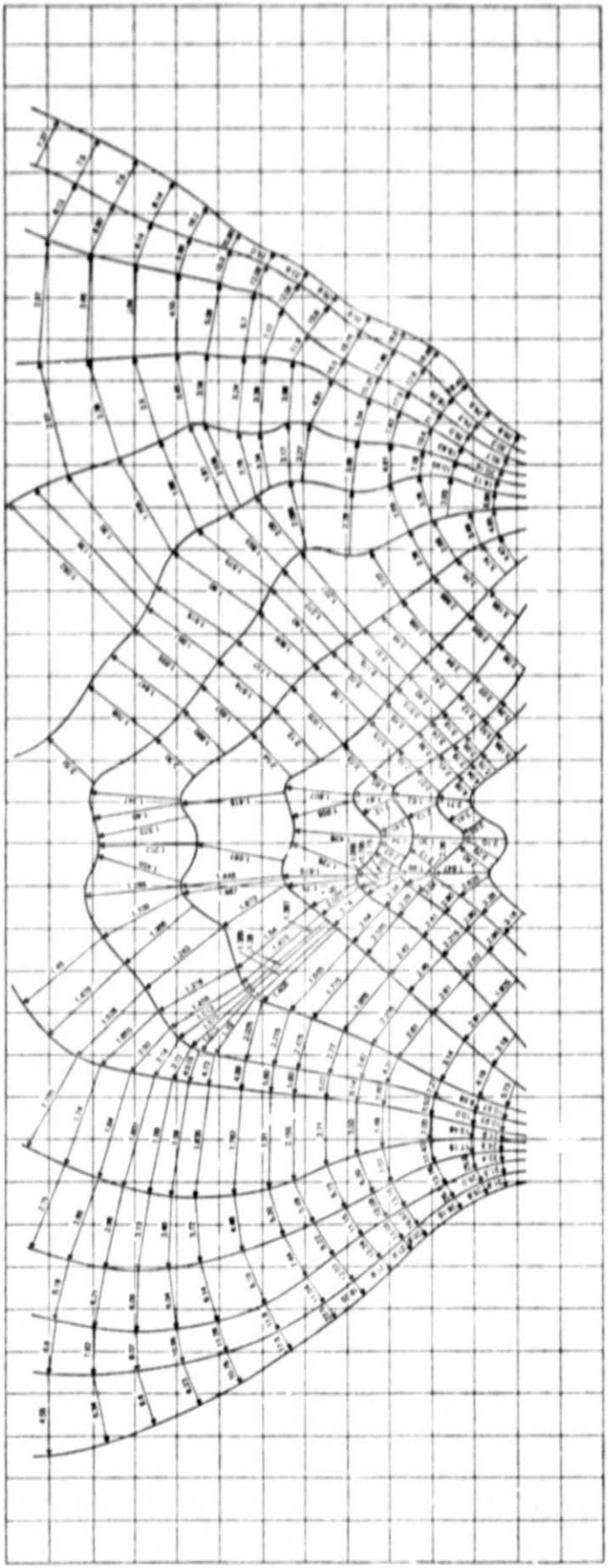

Figure 15. Thrust beam electric field magnitudes (in volts per meter) and directions derived from engine J_+ data (Figure 14), electrostatic barometric relationship, and (assumed) kT_e = 0.35 electron volts.

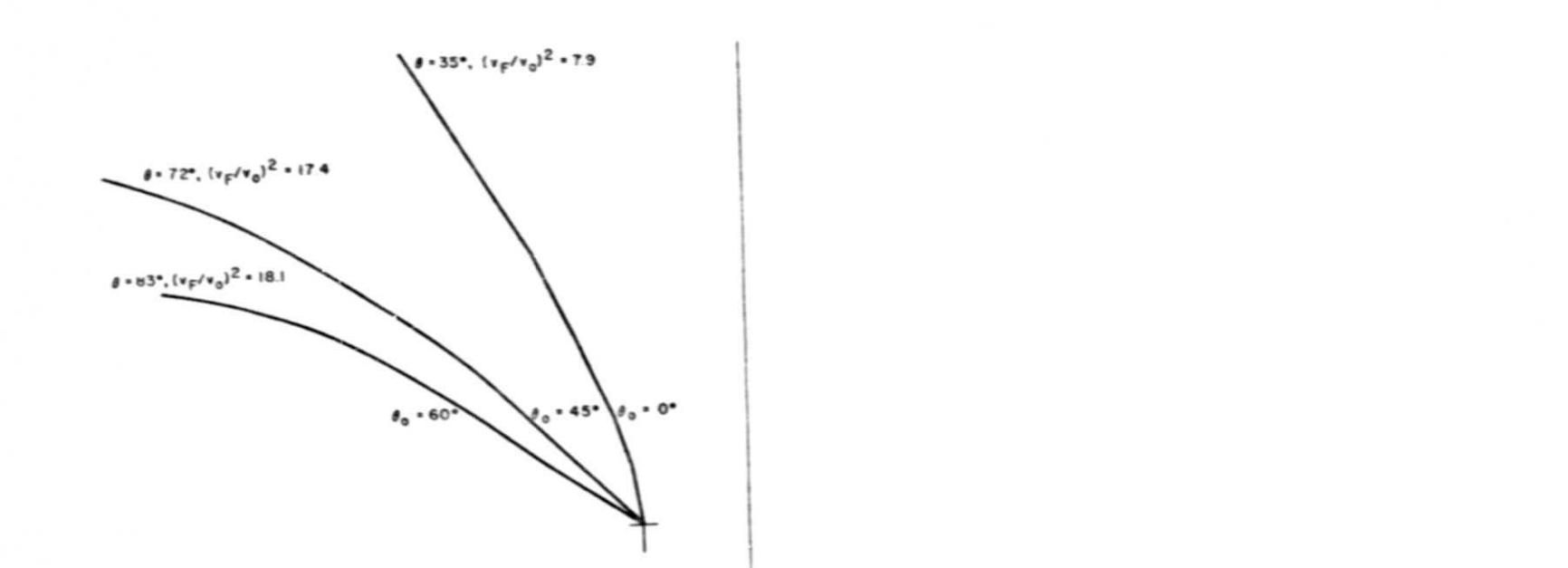

Figure 16. Computed charge exchange ion trajectories derived from thrust beam electric fields (Figure 15) and three initial directions of neutral Hg atom thermal motion (kT = .05 electron volts assumed). Indicated axes are thrust beam axis (r = 0) and accelerator grid plane (z = 0).

5.2 Charge Exchange Conversion Probabilities

The fraction of Hg^o atoms which charge exchange in the reaction

$$Hg^+_{fast} + Hg^o_{slow} \rightarrow Hg^o_{fast} + Hg^+_{slow} \qquad (10)$$

will depend upon the current density and energy of the energetic ions and the "dwell time" of the Hg^o within the regions of high ion flux. If a group of atoms emerge from the ion engine and move along a path of length s, the fraction of the atoms charge exchanging to ions will be given by

$$\eta_{ex} = 1 - \exp\left\{ -\int_o^s \frac{\sigma_{ex} J_+}{v_o} ds \right\} \qquad (11)$$

where σ_{ex} is the charge exchange cross section, J_+ is energetic ion current density (here expressed as particles/cm^2/sec), and v_o is the atom velocity.

To compute η_{ex} the current density of ions along the neutral flight path must be known, and values of σ_{ex} and v_o must be determined. For present modeling purposes, v_o will be the thermal velocity for atoms in equilibrium with surfaces at 500°K. The assumed value of σ_{ex} will be 10^{-15} cm^2. Using these assumptions and the measured J_+ current density patterns (Figure 14), the conversion percentages have been computed for neutrals emerging on the beam axis and at a point 10 centimeters from the beam axis: Figure 17 and 18 illustrates these conversion percentages. Values as high as 1.5% conversion are encountered within z ~ 20 centimeters.

The assumed value of 10^{-15} cm^2 may be an underestimate of the charge exchange cross section. References 3-7 present evidence for values of σ ranging from 2×10^{-15} cm^2 to 8×10^{-15} cm^2, and, if experimental uncertainties should eventually diminish and a value of $Y \times 10^{-15}$ cm^2 can be assigned with reasonable probability to the reaction, then calculated values in Figures 17 and 18 should be multiplied by Y. Viewed alternatively, the conversion fractions given are per 10^{-15} cm^2 of reaction cross section.

The operation of an ion thruster at a total ion current of I_+ and with propellant utilization, η_p, requires a neutral current (equivalent)

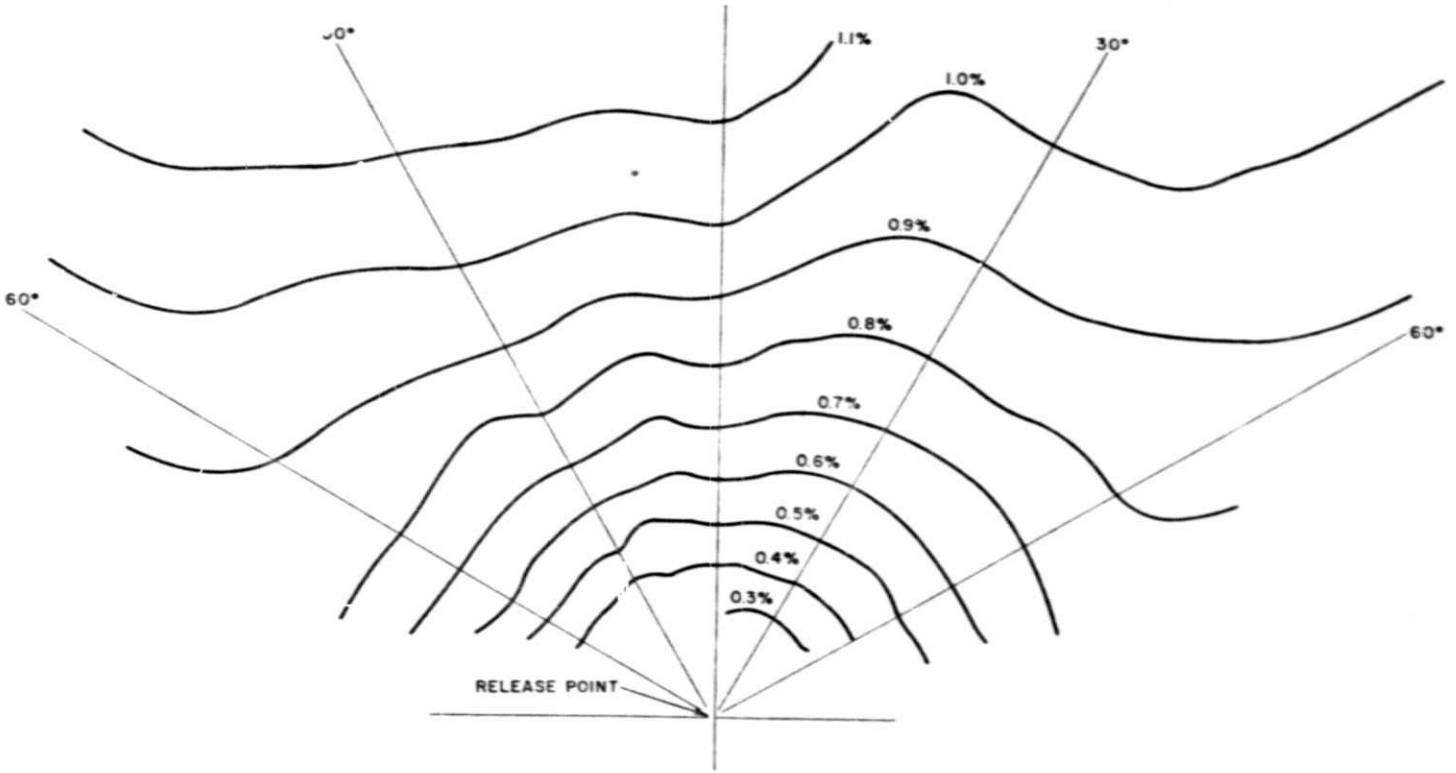

Figure 17. Conversion percentages of Hg atoms to charge exchange ions. Atmos emitted with kT = .05 electron volts at r = z = 0 in the thrust ion flux of Figure 14. Charge exchange cross section of 10^{-15} cm^2 assumed.

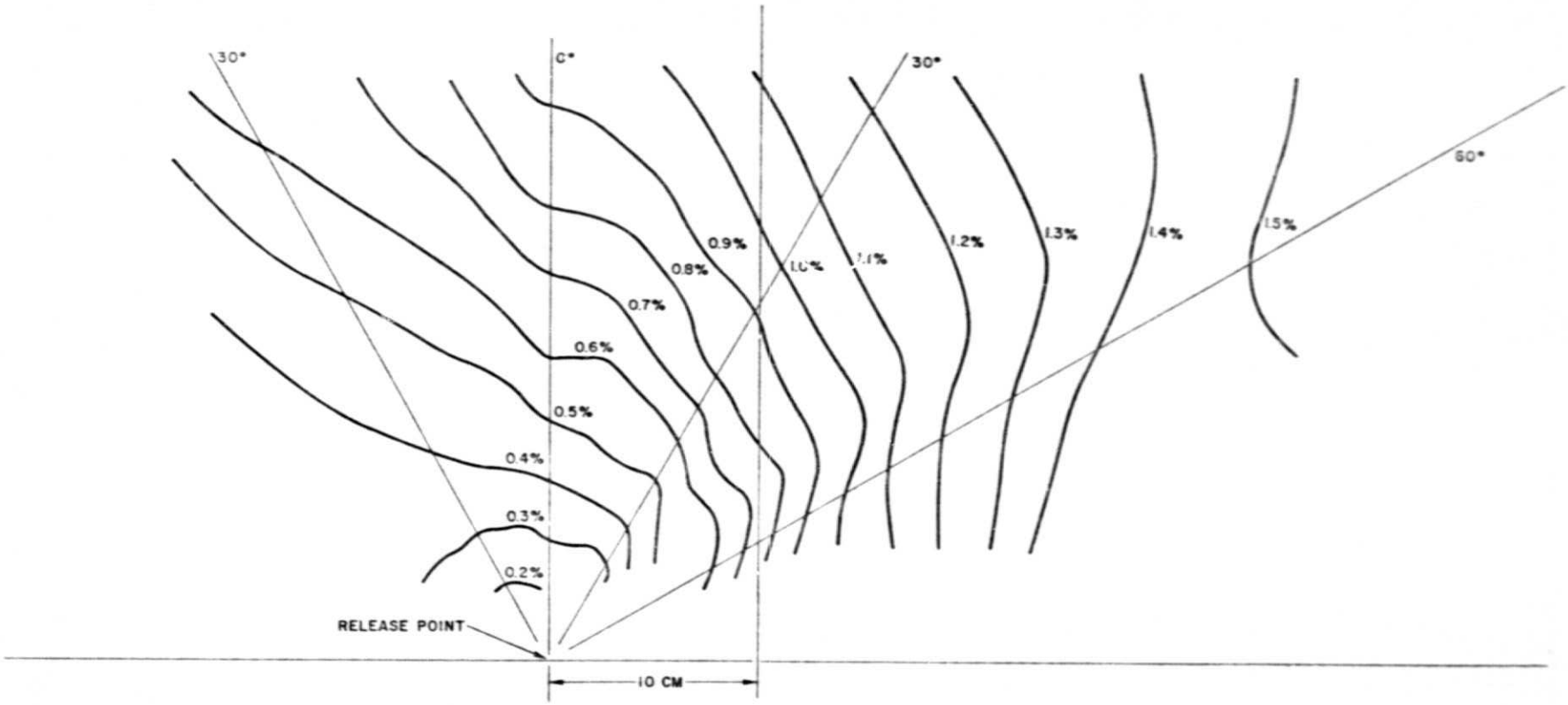

Figure 18. Conversion percentages of Hg atoms to charge exchange ions. Atoms emitted with kT = .05 electron volts at r = 10 centimeters, z = 0 in the thrust ion flux of Figure 14. Charge exchange cross section of 10^{-15} cm^2 assumed.

injection of

$$I_n = \frac{I_+}{\eta_p} \tag{12}$$

of which

$$I_+ \left(\frac{1-\eta_p}{\eta_p}\right)$$

emerges without being ionized. The amount of charge exchange ions formed will be proportional to the product of the released ion and neutral currents,

$$I_{ex} = k\, I_+^2 \left(\frac{1-\eta_p}{\eta_p}\right) \tag{13}$$

and as I_+ reaches "high" levels (large thrusters), charge exchange currents will become significant. Eq. (13) also points out the importance of maintaining η_p as close to unity as practicable. A diminution of η_p from 0.9 to 0.8 causes an increase in I_{ex} (for fixed I_+) by a factor of 2.25.

If values of total ion current and propellant utilization are assigned, net charge exchange currents can be calculated from the data in Figures 17 and 18. For $I_+ = 2.0$ amperes and $\eta_p = 0.9$, the released neutral current would be $\sim$222 milliamperes. The conversion of 2% of these neutrals would lead to a current of $\sim$4.5 milliamperes of charge exchange ions. As these ions move outward and traverse the cylindrical surface along which the 4" J_+ and J_{+W} probes moves ($r \approx 32$ cm), the area over which these ions "deposit" can be estimated as of the order of $10^4 cm^2$ ($2\pi r\Delta z \approx 2\pi(32)(50) cm^2 \approx 10^4 cm^2$). A deposition of $\sim 5 \times 10^{-3} \times 10^{-4}$ amperes per cm^2 would result, using the above charge exchange current. Referring to Figure 9, the summation of the charge exchange ions in all five channels reaches levels of $\sim$400 nanoamperes/cm^2 which is in good agreement with the calculated estimate of $J_{+,ex}$ at 0.5 μamperes/cm^2. It should be emphasized, however, that the J_{+W} probe does not count all charge exchange ions, but only those within the solid angle defined by its collectors and entrance aperture. Also, the estimate of conversion rate may be low, since σ_{ex} may be larger than the figure of $10^{-15} cm^2$ used in the calculations. When these factors are taken into account, estimates of $J_{+,ex}$ along the cylindrical surface discussed may range into the 1 to 2 μampere per cm^2 range.

6. PLASMA POTENTIAL FLUCTUATIONS

The trajectory calculations illustrated in Figure 16 demonstrate how charge exchange ion paths may differ because of initial atom velocity orientation, even for charge exchange ions formed at a single point in the plasma beam. Alternatively, charge exchange ions arriving at a given point in space can differ in their energy and direction depending on the point-of-origin of the ion within the beam. These considerations apply for charge exchange trajectories calculated on a basis of purely steady state electric fields in the plasma column.

If turbulent electric fields exist in the thrust beam, then the action of these fluctuating $\vec{E}$ fields on the charge exchange ions should provide an additional source of angular divergence in the eventual charge exchange ion deposition pattern.

A search for point-to-point fluctuating $\vec{E}$ fields in the thrust beam was not possible within the limited test time of the experiments. However, an examination was made of overall beam potential fluctuations as these potential fluctuations are sensed by the floating potentials of the test chamber shrouds and collector. Figure 19 illustrates these floating potentials and also illustrates the level of fluctuation in the ion engine thrust current.

Three separate examples of thrust ion current fluctuation are given in Figure 19. The ion beam current was 2.0 amperes so that the $\Delta i_+ \sim 0.5$ amperes illustrated there represents a peak-to-peak current fluctuation of $\sim$25%. The characteristic frequency in these current fluctuations is $\sim$5 kilohertz. This same frequency is evident in the fluctuations of plasma potential. Three examples of collector floating potential reveal peak-to-peak fluctuations of $\sim$1 volt. When the floating potentials of the upper and lower shrouds are viewed simultaneously (two examples) and the floating potentials of the lower shroud and the collector are viewed simultaneously (two examples) it is evident that the potential excursions of the shrouds and the collector occur at the same time and with the same magnitude. Thus, at least, the major portion of the flucutaions in plasma beam potential are "common mode" (entire plasma column moving together) and are coupled to initial fluctuations in ion

ION BEAM CURRENT

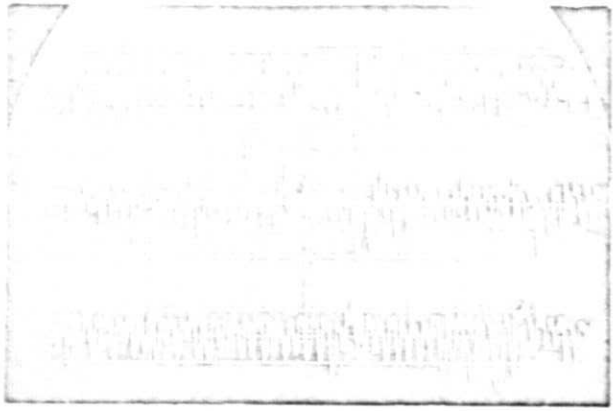

Vertical: 0.5 Amp/div

Horizontal: 1 msec/div

FLOATING POTENTIALS

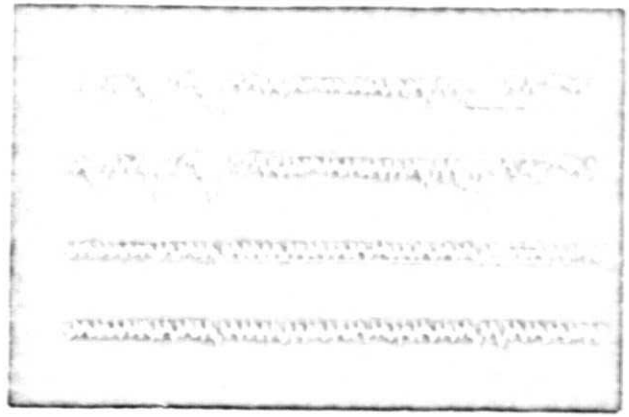

A. UPPER SHROUD

B. LOWER SHROUD

C. UPPER SHROUD

D. LOWER SHROUD

Vertical: 2 volts/div

Horizontal: 1 msec/div

COLLECTOR FLOATING POTENTIAL

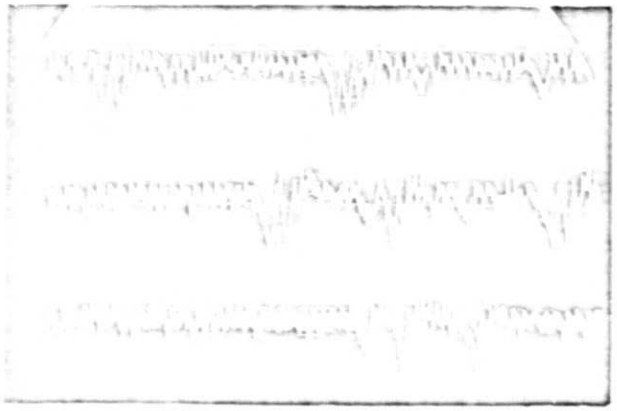

Vertical: 2 volts/div

Horizontal: 1 msec/div

FLOATING POTENTIALS

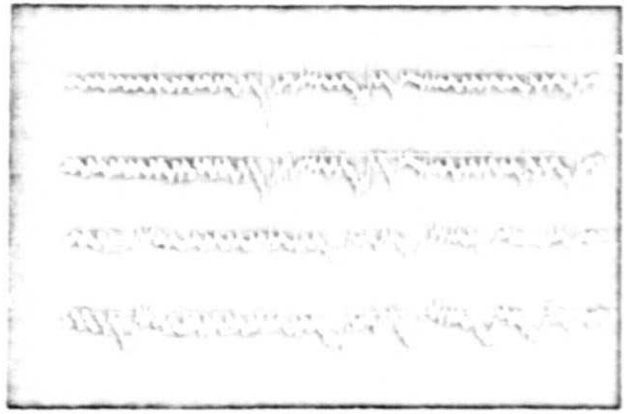

A. LOWER SHROUD

B. COLLECTOR

C. LOWER SHROUD

D. COLLECTOR

Vertical: 2 volts/div

Horizontal: 1 msec/div

Figure 19. Temporal fluctuations of thrust ion current and floating potentials of upper and lower chamber shrouds and ion beam collector.

beam current. This does not demonstrate, however, an absence of point-to-point electric fields, and the determinations of the levels of these fields will be of importance in assessing turbulent field angular dispersion of the charge exchange ions emerging from the beam.

7. HIGH ANGLE HIGH ENERGY ION CURRENTS

Currents of ions are observed on the J_{+W} collectors in both the forward and backward hemispheres and with energies well in excess of charge exchange ion energies. Retardation potentials at the 150 volt level diminished these currents somewhat but not totally.

In describing these currents some general order of magnitude characterizations will be of value. The logical unit in descriptions of the thrust ion current densities is in milliamperes per cm^2. The logical unit in charge exchange ion current densities, as viewed at the probe locations, is micoramperes per cm^2. For the energetic high angle ions, a logical unit is in nanoamperes per cm^2.

Some fraction of these currents may be originated by "facility effects" (near presence of material boundaries). In view of the many orders of magnitude between thrust beam current and high angle energetic ions, some fraction of these currents may be of genuine (beam) origin. Further definition of the particles in energy, magnitude, and mode of creation should be carried out in order to assess possible impact resulting from the interaction of the particles on spacecraft surfaces.

8. SUMMARY

A series of experiments have been performed with a 30-cm diameter ion engine. The thrust ions of the beam are comparatively broad, but ion flow patterns are not unexpected in view of the screen and accelerator grid hole sizes and the absence of compensation in the grids utilized.

The magnitudes and directional properties of the charge exchange ions have been examined. A model of the thrust beam - neutral atom - charge exchange formation and deposition is in qualitative agreement with experimental results on current density magnitudes and current deposition patterns.

The observed angular divergence of the charge exchange ions is broad and may not be derivable from the model which utilized only steady state electric fields in its formalism.

"Common mode" fluctuations of plasma beam potential have been observed. Detailed searches for point-to-point turbulent electric fields which could be the source of additional charge exchange ion angular divergence were not carried out in the present measurements, and should be conducted.

Small currents of energetic high angle ions were observed and may result from genuine thrust beam interactions. Further experimental definition of these particles should be carried out.

The magnitude of the total charge exchange current from the beam is of the order of milliamperes. Control and minimization of these currents should be examined in detail in view of particle current levels.

REFERENCES

1. "Measurement of Beam Divergence of 30-Centimeter Dished Grids", R. L. Danilowicz, V. K. Rawlin, B. A. Banks, and E. G. Wintucky, Presented at the AIAA 10th Electric Propulsion Conference, Lake Tahoe, Nevada, October 31 - November 2, 1973. AIAA Preprint 73-1051.

2. "Solar Electric Propulsion/Instrument/Subsystem Interaction Study", J. M. Sellen, Jr., R. K. Cole, R. F. Kemp, D. F. Hall, and H. Shelton, Final Report NAS2-6940, TRW 22878-6007-RU-00, 30 March 1973.

3. "Charge Transfer Reactions in Monatomic and Diatomic Gases", J. A. Dillon, W. F. Sheridan, H. D. Edwards, and S. N. Ghosh, Journal Chem. Physics, 23, 776-779, 1955.

4. "Charge Exchange Between Gaseous Ions and Atoms", Donald Rapp and W. E. Francis, Journal Chem. Physics, 37, 2631-2645, 1962.

5. "Measurement of the Charge Exchange Cross Section of Mercury", David Zuccaro, Final Report Contract NAS 3-7932, NASA CR-72398, August 1967.

6. "Charge Transfer Cross Sections and Mobilities for Hg^+ Ions in Atomic Mercury", J. C. McConnell and B. L. Moiseiwitsch, Journal Physics B, Series 2, Vol. 2, 821-830, 1969.

7. "Charge-Exchange Calculations with Hartree Wavefunctions", I. Nebenzahl, Journal Chem. Physics, 54, 5254-5256, 1971.